



Published in final edited form as:

J Microsc. 2008 January ; 229(Pt 1): 21–31. doi:10.1111/j.1365-2818.2007.01870.x.

Automated assessment of keratocyte density in clinical confocal microscopy of the corneal stroma

J. W. McLAREN, S. V. PATEL, C. B. NAU, and W. M. BOURNE

Department of Ophthalmology, Mayo Clinic College of Medicine, 200 First Street SW, Rochester, MN 55905

Summary

Cell density in the corneal stroma is typically determined by counting the number of bright objects, presumably keratocyte nuclei, in images from clinical confocal microscopy. We present a program that identifies bright objects and counts those that most likely represent cells. Selection variables were determined from 125 normal corneas with cell densities that had been assessed manually. The program was tested on 17 corneas of patients before and at several intervals to 5 years after laser in situ keratomileusis (LASIK) surgery. In these corneas, which showed a decrease in cell density after surgery, the program identified cells as well as human observers did.

Keywords

cell density; confocal microscopy; cornea; image processing; keratocyte density; keratocyte

Introduction

Keratocytes are fibroblast-like cells that maintain the health and clarity of the corneal stroma. Several investigators have examined changes in density of these cells with age (Moller-Pedersen, 1997; Mustonen *et al.*, 1998; Hollingsworth *et al.*, 2001; Patel *et al.*, 2001; Berlau *et al.*, 2002), with contact lens wear (Jalbert & Stapleton, 1999; Efron *et al.*, 2002a, b; Patel *et al.*, 2002; Kallinikos & Efron, 2004; Kallinikos *et al.*, 2006), after refractive surgery (Frueh *et al.*, 1998; Erie *et al.*, 1999; Moller-Pedersen *et al.*, 2000; Vesaluoma *et al.*, 2000; Pisella *et al.*, 2001; Mitooka *et al.*, 2002; Erie, 2003; Erie *et al.*, 2003, 2004, 2006; Perez-Gomez & Efron, 2003), and after corneal transplantation (Bourne, 2001; Mikek *et al.*, 2003; Imre *et al.*, 2005). These studies all required non-invasive and accurate estimates of keratocyte density in corneas of study subjects and patients.

Keratocyte nuclei scatter and reflect a small amount of light and are sometimes visible during slit lamp examination (Moller-Pedersen, 2004), although they are more prominent in clinical confocal images of the stroma. Keratocyte density in human corneas has been estimated from confocal images by counting the number of bright objects (assumed to be keratocyte nuclei) in a field of known area and dividing by the sample volume, the area multiplied by the effective depth of field (Patel *et al.*, 1999; Popper *et al.*, 2004; McLaren *et al.*, 2005), although Berlau and coworkers (2002) estimated density from the number of cells distributed through several frames. Some investigators have reported cell density in terms of cells per unit area for a

particular confocal microscope (Frueh *et al.*, 1998; Mustonen *et al.*, 1998; Prydal *et al.*, 1998; Jalbert & Stapleton, 1999; Vesaluoma *et al.*, 2000; Hollingsworth *et al.*, 2001; Pisella *et al.*, 2001; Perez-Gomez & Efron, 2003; Vanathi *et al.*, 2003).

The accuracy and precision of manually counting cell nuclei depends on the ability of the observer to discriminate nuclei from the background noise in the image and to interpret the variable appearance of cell nuclei located at different depths within the optical section of the image. Nuclei with the highest contrast and sharpest edges can be consistently identified, whereas those with lower contrast and blurred edges will be inconsistently identified. Because of this subjectivity, two investigators, or one investigator assessing density in the same images on two sessions, rarely arrive at exactly the same density (McLaren *et al.*, 2001).

A program that identifies and selects cells in confocal images would be more objective than manual assessment of low-contrast images. Programs that count keratocytes have been reported (Prydal *et al.*, 1998; Patel *et al.*, 1999), but none have been used consistently in clinical studies. Patel *et al.* (1999) described and histologically validated an automated algorithm to estimate keratocyte density in rabbit corneas. However, this method did not work consistently in human corneas and its use has not been demonstrated in a longitudinal study.

In this study, we further developed and refined the algorithm described by Patel *et al.* (1999) and tested it in confocal images of the human corneal stroma. Cell densities determined by the automated method were compared to densities determined by manually counting keratocyte nuclei in the same images, in a population of patients who received laser in situ keratomileusis (LASIK) and experienced a decrease in cell density.

Methods

Human subjects

All human subjects were participants in other studies in our laboratory, and these studies have been described in other papers. Image variables used in the cell-counting program were defined from confocal scans of 125 corneas of 79 subjects. This sample included 30 normal control corneas of 19 subjects from a study of keratoconus (Erie *et al.*, 2002), 25 pre-operative corneas of 15 patients who received photorefractive keratectomy (PRK) (Erie *et al.*, 1999), 20 corneas of 20 subjects in a study of contact lens wearers (Patel *et al.*, 2002) and 50 corneas of 25 subjects in a study of corneal thickness (Kitzmann *et al.*, 2005; McLaren *et al.*, 2005). Scans were acquired between July, 1998 and July, 2003, and images from these scans were used to define selection criteria in the cell-counting program. The program was tested by assessing cell density in another group of 17 corneas from 11 patients before and at several intervals after LASIK through 5 years (Mitooka *et al.*, 2002; Erie *et al.*, 2004, 2006). All subjects were examined before the study to assure that their corneas and anterior segments were normal. Each subject gave informed consent to participate in the study after the nature and possible consequences of the study had been discussed. All studies were approved by the Institutional Review Board of Mayo Clinic and conformed to the tenets of the Declaration of Helsinki for research involving human subjects.

Confocal microscopy

Corneas were scanned by using a clinical tandem scanning confocal microscope (Tandem Scanning Corporation, Reston, Virginia, U.S.A.), by methods that have been described in detail previously (Patel *et al.*, 1999, 2001). Briefly, the cornea was anaesthetized by instilling topical proparacaine 0.5%, a drop of a viscous coupling solution (Goniak; Akorn Inc., Buffalo Grove, IL, or GenTeal Gel; Novartis Ophthalmics, East Hanover, New Jersey) was placed on the tip of the objective lens, and the objective lens was advanced until this solution contacted the

cornea. The objective lens was aligned with the centre of the cornea by centring the light and dark rings in the image of the epithelial surface. The focal plane of the microscope was retracted to inside the objective surface, and then advanced through the cornea at approximately $72 \mu\text{m s}^{-1}$ while video images were digitized and stored by a computer at 30 frames s^{-1} . The video camera automatically adjusted its gain to maintain a constant image brightness.

Manual assessment of cell density

Each confocal scan through the stroma was reviewed and 10-12 frames were selected that had clear, non-blurred images of cell nuclei and did not have signs of motion artifacts. In control corneas, two frames were selected in each of five layers of the stroma, the anterior 0-10%, 10-33%, 33-66%, 66-90% and 90-100% of stromal depth (Patel *et al.*, 2001). In corneas after LASIK, two frames were selected in the anterior and posterior half of the flap, the anterior and posterior halves of the region that extended 100 μm deep to the ablated surface, and the regions represented by 66-90% and 90-100% of the pre-LASIK stromal depth (Mitooka *et al.*, 2002). Frames from the equivalent regions of stroma were selected from scans before LASIK.

Cell density was assessed manually by counting bright objects that were presumed to represent keratocyte nuclei inside a pre-defined rectangle ($379 \mu\text{m}$ by $286 \mu\text{m}$) by using a simple point-and-click method. Objects that touched the bottom or left edge of the rectangle were counted, but objects that touched the top or right edge were not counted. Each object was marked with an 'X' to prevent double counting. Frames from each cornea were presented to the investigator in random order so that the investigator was masked to the depth of the frame in the stroma and the identity of the subject. Cell density was expressed as cells mm^{-3} :

$$\text{Density} = \frac{N}{A\delta} \quad (1)$$

where N is the number of objects counted, A is the area of the selection rectangle, and δ is the effective depth of field, (the full-width-at-half-maximum of a scan through a reflecting surface plus the mean axial thickness of a keratocyte nucleus) (Patel *et al.*, 1999; McLaren *et al.*, 2005). We assumed $A = 0.109 \text{ mm}^2$ and $\delta = 0.0119 \text{ mm}$ (McLaren *et al.*, 2005). One investigator (CBN) assessed cell densities in all confocal images from the study of LASIK patients. Cell densities in the four groups of normal subjects were assessed by three investigators: pre-PRK and controls for the keratoconus study by one investigator, contact lens control corneas by another, and the corneal thickness study by a third (CBN).

Automated assessment of cell density

A program was developed to assess cell density in confocal images by using a scripted language, Tcl/tk ("tool command language/toolkit," www.tcl.tk), and an image processing program, Analyse AVW (Mayo Medical Ventures, Rochester, Minnesota). The program worked in two steps; first, it identified bright objects in the field, and second, it selected those objects that most likely corresponded to cells based on the image properties of each object.

The algorithm that identified bright objects was similar to the process described by Patel, *et al.* (1999), although several steps were added to separate cell nuclei that overlapped each other. The original image processing steps are given in Table 1, and the additional steps used to separate overlapping objects are listed in Table 2. These steps created a binary mask of all bright objects in the frame. The mask of each object was isolated one at a time and the area around the object (background) was identified by creating a second mask as a band, approximately 11 pixels ($8.6 \mu\text{m}$) wide and separated by a 5-pixel gap ($3.9 \mu\text{m}$) from the object mask. Portions of the background mask that overlapped masks of other cells were excluded. The program calculated several variables including object size, mean and standard deviation

of intensity of the object and background, minimum and maximum brightness, and coordinates of the geometric centre, from the areas in the original and processed images defined by the masks of the object and background. Contrast and brightness-area-product (BAP) of each object relative to the background brightness were calculated:

$$\text{Contrast} = \frac{I_c - I_b}{I_b} \quad (2)$$

$$\text{BAP} = (I_c - I_b) A_c \quad (3)$$

where I_c and I_b are the mean intensities of the cell and background respectively, calculated from the inhomogeneity-corrected image (step 1 in Table 1), and A_c is the area of the cell. After several preliminary trials of images from our control group, we found that cell contrast and BAP were the best variables for selecting objects that the human observers would most likely have identified as cells. The original program used by Patel *et al.* (1999) selected cells based on size; objects greater than a pre-determined size were counted as cells.

The program examined the image properties of each object and it selected objects with contrast greater than 0.03 and BAP greater than a pre-set threshold. The selected objects were counted as cells if they were entirely inside of a rectangle similar to that used in manual assessment (367 μm by 277 μm) or overlapping the left or bottom edge of the rectangle. Cell density was determined by using Eq. (1) (McLaren *et al.*, 2005).

The optimum BAP threshold (BAP_{thr}) was determined from ten frames in each of 125 confocal scans from our control group. Cell density in each frame was assessed manually. The BAP threshold that forced the program to estimate the same density as the manual assessment was determined iteratively for each frame, and the mean threshold of the ten frames ($\overline{\text{BAP}}_{\text{thr}}$) was calculated for each scan. When the mean background intensity after the adaptive histogram equalization step ($I_{b\text{-ahe}}$) was above a specific value ($I_{b\text{-min}}$), the $\overline{\text{BAP}}_{\text{thr}}$ decreased as $I_{b\text{-ahe}}$ increased. The optimum BAP threshold for a particular frame also varied with depth in the stroma.

In addition, five scans from the LASIK patients at each visit at 1, 3, 6 and 12 months after LASIK were randomly selected and used to determine $\overline{\text{BAP}}_{\text{thr}}$. During the first post-operative year $I_{b\text{-ahe}}$ was elevated compared to that from scans in control subjects. Selection of a subset of scans from the LASIK patients was necessary to include the full range of $I_{b\text{-ahe}}$. During this interval, scans were not available from control subjects who did not participate in the LASIK study.

The program used the BAP threshold to determine which objects most likely represented cells. The BAP_{thr} was selected in two steps, selection of the $\overline{\text{BAP}}_{\text{thr}}$ for the scan and selection of the specific BAP_{thr} for the frame. The program selected $\overline{\text{BAP}}_{\text{thr}}$ based on the value of $I_{b\text{-ahe}}$. If $I_{b\text{-ahe}}$ was less than $I_{b\text{-min}}$, then $\overline{\text{BAP}}_{\text{thr}}$ was set to a constant, but if it was greater than or equal to $I_{b\text{-min}}$, $\overline{\text{BAP}}_{\text{thr}}$ was determined by:

$$\overline{\text{BAP}}_{\text{thr}} = I_{b\text{-ahe}} \times m_1 + b_1 \quad (4)$$

where m_1 and b_1 are constants determined by linear regression of \overline{BAP}_{thr} and $\overline{I_{b-ahc}}$.

The BAP threshold for the i^{th} frame (BAP_{thr-i}) was selected in a second step:

$$BAP_{thr-i} = \overline{BAP}_{thr} \left(\frac{\overline{I_{b-ahc-i}}}{\overline{I_{b-ahc}}} \times m_2 + b_2 \right) \quad (5)$$

where $\overline{I_{b-ahc-i}}$ is the mean intensity of the background regions after adaptive histogram equalization in the frame, and m_2 and b_2 are constants determined by regression.

The constants m_1 , b_1 , m_2 and b_2 were determined from confocal scans of the 125 normal corneas, and b_2 was increased or decreased slightly to further optimize agreement between densities determined manually and automatically.

Cell density in LASIK patients

Cell density was estimated manually and by using the automated method in 17 corneas from 11 patients before and at 1, 3 and 6 months, and at 1, 2, 3 and 5 years after LASIK. These were different corneas than those used to define the constants in Eqs (4) and (5), except for the subjects randomly selected at 1, 3 and 6 months, and 1 year as described in the previous section. The mean of cell densities determined from the two frames from each layer was accepted as the cell density of the layer, and the mean cell density of each cornea was the mean cell density from all six layers, unweighted for the thickness of the layer.

Differences between the estimate of mean cell density of each cornea by the automated and the manual methods were assessed by using generalized estimating equation models, to account for the possible correlation between eyes of the same subjects, at each visit (pre-LASIK through 5 years). Tests were considered significant if $P < 0.05$. The minimum detectable difference was calculated for each non-significant difference by using the standard error from the generalized estimating equation models, and assuming $\alpha = 0.05$ and $\beta = 0.20$. Mean cell densities in each layer after LASIK, determined by manual and automatic assessment, were compared to densities in the same layer before LASIK by using generalized estimating equation models. Significances were adjusted for seven comparisons by using the method of Bonferroni.

Repeatability of manual assessment

Densities in 276 frames from 23 corneas at 2 and 3 years after LASIK were assessed manually a second time, and the correlation coefficient of concordance (Lin, 1989), mean difference and limits of agreement, the mean difference ± 2 standard deviations of the mean as described by Bland & Altman (1986), between the first and second assessment were determined. Of these, 108 images from nine corneas at 3 years after LASIK were assessed a third time. Mean densities estimated in the three assessments were compared to each other and to automated density estimates by using paired t-tests.

Results

A typical confocal image from the mid-stroma is shown in Fig. 1. The inset shows two bright objects and their corresponding cell and background masks as identified by the program. Figure 2 shows a mid-stromal frame with manual identification of cell nuclei marked with X's and automatic identification noted by bounding boxes. Not all objects identified by the observer were identified by the program as cell nuclei, and not all objects identified by the program were identified by the observer. The program required approximately 18 s to assess each frame,

while manual assessment required 35-85 s (not including breaks in the work and time between scans required to load the new file), depending on the scan.

Selection parameters

The relationship between \overline{BAP}_{thr} and $\overline{I_{b-ahc}}$ is shown in Fig. 3. The specific \overline{BAP}_{thr} selected by the program is shown as a solid line, and the coefficients of the selection line (Eq. 4) are given in Table 3. The coefficients of Eq. (4) changed after March 1999, a time when the video system was adjusted to optimize the image. The appropriate parameters, depending on the date of the scan, were used with Eq. (4) to determine \overline{BAP}_{thr} for each scan.

The relationship between the \overline{BAP}_{thr-i} and $\overline{I_{ahc-i}}$ normalized to \overline{BAP}_{thr} and $\overline{I_{b-ahc}}$ is shown in Fig. 4. The constants used in Eq. (5) determined from these data were $m_2 = 7.652$ and $b_2 = -6.667$ before March, 1999, and $m_2 = 5.477$ and $b_2 = -4.529$ after March, 1999.

Cell density in control corneas

The mean cell density, unweighted by thickness of the layer, from all corneas used to determine selection parameters, was 28614 ± 10608 cells mm^{-3} by manual assessment and 28251 ± 9452 cells mm^{-3} by automatic assessment (\pm SD, $n = 1247$ frames). The mean difference was -363 ± 5214 cells mm^{-3} (automatic - manual, $P = 0.014$). In the first frame (anterior stroma) of the pre-PRK group of patients, the mean difference between densities by manual and automatic methods was -16320 cells mm^{-3} and was greater than mean differences in any layer for any other group. The next smaller difference was less than 5000 cells mm^{-3} . When this first frame from the pre-PRK group was excluded, the mean densities of all other frames by manual and automatic assessments were 28088 ± 9939 cells mm^{-3} and 28051 ± 9373 cells mm^{-3} respectively, and the difference was -37 ± 4518 cells mm^{-3} ($n = 1222$ frames, $P = 0.78$).

Cell density before and after LASIK

The mean cell densities before and after LASIK, determined by both methods, are given in Table 4. Mean cell densities determined by the two methods were within 7.2% of each other throughout the 5 years of the study.

Significances of differences at each visit with cell density before LASIK are shown in Table 5 for each of six layers for manual and automated methods. The pattern of significance by automated assessment was similar to that of manual assessment; cell density was decreased in the flap at all post-LASIK examinations. Density decreased significantly just posterior to the interface (anterior retro-ablation zone) by the automated method at 1 year and later, while according to the manual method significant differences in this region persisted at all measurements after LASIK. The manual method also detected a few differences that the automated method did not, particularly at 3 and 5 years. Manual assessment had slightly more statistical power; the average minimum detectable difference for the comparisons that were not significant was 3932 cells mm^{-3} with manual assessment and 4219 cells mm^{-3} with automated assessment.

An example of the relationship between manual and automatic assessments of cell densities at the 5-year visit is shown in Fig. 5. The correlation coefficient of concordance was 0.83 (95% confidence interval: 0.79-0.87; Fig. 5A). The mean difference between methods at 60 months was 1392 ± 3881 cells mm^{-3} and limits of agreement for this example were -6371 - 9154 cells mm^{-3} (Fig. 5B).

Repeated manual assessment

Mean cell densities assessed manually three times in the same frames differed from each other by as much as 3160 cells mm⁻³ (Table 6). Differences between these three manual assessments and the automatic assessment ranged from -1286 cells mm⁻³ to 1874 cells mm⁻³. The relationship between cell densities at 2 and 3 years assessed twice by the same observer is shown in Fig. 6. The correlation coefficient of concordance between the first and second assessment was 0.86 (95% confidence interval: 0.83-0.89; Fig. 6A). The mean difference was 2358 ± 3219 cells mm⁻³ ($P < 0.001$) and limits of agreement ranged from -4082 to 8797 cells mm⁻³ (Fig. 6B).

Discussion

This program for identifying and counting cells in confocal images of the cornea expands the scope of earlier attempts at estimating cell density automatically. It has a refined algorithm for separating overlapping objects and uses dynamic selection of criteria for discriminating cells from other objects. Selection criteria are based on measurements from each image, and these criteria may vary as characteristics of the microscope and video system vary. The program was designed to emulate a human observer, and the assessment of the large data set from our study of LASIK patients demonstrates that we would have reached a similar conclusion by using the program to assess cell density as we did with manual assessment. Repeatability is the greatest advantage of this program; results will not differ from one assessment to the next as they can with manual assessment. Use of the program also reduces time needed to determine cell density.

Repeatability and accuracy of cell density

Manual assessment of corneal stromal cell density from a clinical confocal image is subjective. An investigator who estimates cell density will rarely identify all of the same objects on repeated assessments of the same frames (Fig. 6). Similarly, two observers who estimate cell density may arrive at considerably different mean densities. Variability from imperfectly identifying all cells in an image determines in part the minimum detectable difference of this measurement in a study.

The subjectivity of manual assessment is partially caused by low contrast between the objects in the field and their background, poorly defined object boundaries, or indistinct texture within an object. Most cell nuclei in a typical stromal image are clearly distinguishable and are identified consistently. However, some nuclei, particularly if they are located near the edge of the focal depth of field, have low contrast or other poorly distinguishing features. An observer might identify low-contrast objects as cell nuclei in one session and as background noise in another session.

A program that uses image processing has the advantage of objectively identifying cell nuclei by using numeric properties of the image. Criteria for identifying cells will always be consistent from frame to frame and subject to subject, and if the image properties remain constant, selection of cells will be consistent, and this is the greatest advantage of using a program for determining cell density. When the image properties changed in our study because of alterations on the microscope, the program was able to select the appropriate BAP threshold based on the image variable I_{b-ahc} .

The differences between cell densities determined by the program and those determined manually in the same frames were similar to differences between cell density assessed twice by the same investigator (Fig. 5, Table 4). These differences could be attributed to variability in identification of cells by the observer, particularly if many of the cell images are near the limit of visibility.

In spite of these differences, we would have arrived at the same general conclusions concerning the decrease in cell density after LASIK if we had used the program as we did with manual assessment (Table 5). In the flap (layers 1 and 2) densities were decreased significantly by both methods at all times after treatment. In the deeper layers of the stroma the manual method indicated more differences in cell density that were significant, particularly at 3 and 5 years. This is likely a consequence of the slightly lower minimum detectable differences (greater statistical power) that we noted in the manual assessments.

Sources of error

Accurate estimates of cell density, either by manual or automated methods, require high-quality images. Any characteristic that degrades the image, such as poor contrast between cells and background, distortion because of lateral or axial motion, position of the cell near the axial limits of the field, or optical or electronic image noise that degrades boundaries, will render cells less visible and increase the probability that they will be missed by an observer. In the program, the same features could alter the selection variables used by the program and degrade the identification of cells. It is not possible to predict how a particular image change might affect an observer's ability to identify cells relative to the program's ability.

Changes in the image properties of the confocal microscope were likely the source of our need to adjust the coefficients of Eqs (4) and (5) after March, 1999. The relationship between the image properties and BAP threshold changed after we had adjusted the microscope and video electronics to optimize the quality of the image. This demonstrates the importance of stability of the confocal images and periodic checks for agreement with manual assessment, particularly after a known adjustment to the microscope. Any change in image characteristics that affects the relationship between the BAP threshold and I_{b-ahc} could lead to erroneous cell density estimates unless the changes are considered. The equations and coefficients we used to determine BAP threshold are specific for our confocal microscope, and although the principles that we describe can be applied to other systems, the specific selection parameters must be determined for the individual system.

Our model for selecting BAP threshold worked well when we used this method to determine cell density before and after LASIK. At best, this method is only as accurate as our ability to assess cell density manually, however, because the program was designed to emulate manual assessment. This approach is justified by earlier studies where manual assessments of density from confocal images agreed with densities determined histologically in the same corneas (Patel *et al.*, 2001).

Cell densities in one set of images were consistently underestimated by the program, the frames of the anterior-most keratocytes in the pre-PRK subjects. We do not know why these frames were different from others recorded at different times, although the confocal microscope was operating under somewhat different video parameters than it was later, as indicated by the change in selection criteria noted in Table 3. In spite of this mismatch, the program performed well on frames from the same region of stroma in the pre-LASIK patients, images that were recorded at approximately the same time. Differences between manual and automatic methods were not associated with other image variables, such as cell contrast, cell intensity, or I_{b-ahc} .

The variability of the BAP threshold and its relationship with the image parameter I_{b-ahc} demonstrates the importance of defining the selection parameters for a particular microscope and camera and any video controls that must be set. Other clinical confocal microscopes, such as the ConfoScan 4 (Nidek Technologies, Srl., Padova, Italy) and the Heidelberg HRT-II with the Rostock Corneal Module (Heidelberg Engineering GmbH, Dossenheim, Germany), produce images with greater contrast between nuclei and background than the Tandem Scanning confocal microscope does. In principle, cell densities determined from these images

should be more consistent between automated and manual assessment than from images recorded by microscopes that produce low-contrast images. However, variables used with images from other microscopes to optimize object and cell identification will likely be different from those used in the present study to optimize object identification. Cell selection criteria must be determined or verified by using an independent method of density assessment, such as manually counting cells in a standard image area.

One must recognize that criteria for cell identification may be altered in corneas that are abnormal or have been manipulated as compared to images from normal corneas. For example, if a treatment brings the refractive index of keratocyte nuclei closer to that of the surrounding substance, cell nuclei would become less visible as suggested by Efron *et al.* (2002a) after overnight contact lens wear. The ability to identify these cells would diminish and the apparent cell density could decrease for both manual and automated assessment. Our best verification of cell density would be to compare density determined by confocal microscopy to that determined by histology in the same tissue. However, this is not an option in most studies, and the next best standard is manual assessment, although as we have shown, manual assessment is variable. Our program is capable of working at least as well as manual assessment in normal and post-LASIK corneas.

Frame selection

In clinical confocal microscopy, some frames are degraded by motion. In these frames, bright objects including cells appear elongated in the direction of movement and faint objects often cannot be distinguished from the background. We selected frames that contained objects with sharp edges and did not show these motion artifacts before we assessed density manually. The automatic selection of high-quality frames for automatic cell density assessment will be another refinement of this program.

In summary, we present an algorithm that identifies bright objects in confocal images of the corneal stroma *in vivo*. The program was designed to emulate a human observer and its utility was demonstrated by assessing cell density in the same images that were assessed manually in a longitudinal study of LASIK patients. The program detected similar changes in cell density as the manual observer did and we would have arrived at a similar conclusion had we used the automated method. This objective method will improve the repeatability and accuracy of cell density assessment in clinical confocal images of the cornea. The principles of this algorithm can be applied to identifying low-contrast objects in images from other microscopy systems.

Acknowledgement

The authors thank Jon J. Camp, Biomedical Imaging Resource at the Mayo Clinic College of Medicine, for many helpful discussions and for writing the first version of this program.

Supported in part by NIH grant EY 02037 (WM Bourne), Research to Prevent Blindness, Inc., New York, NY, and Mayo Foundation, Rochester, MN.

References

- Berlau J, Becker HH, Stave J, Oriwol C, Guthoff RF. Depth and age-dependent distribution of keratocytes in healthy human corneas: a study using scanning-slit confocal microscopy *in vivo*. *J. Cataract Refract. Surg* 2002;28:611–616. [PubMed: 11955900]
- Bland JM, Altman DG. Statistical methods for assessing agreement between two methods of clinical measurement. *Lancet* 1986;1:307–310. [PubMed: 2868172]
- Bourne WM. Cellular changes in transplanted human corneas. *Cornea* 2001;20:560–569. [PubMed: 11473153]

- Efron N, Mutalib HA, Perez-Gomez I, Koh HH. Confocal microscopic observations of the human cornea following overnight contact lens wear. *Clin. Exp. Optom* 2002a;85:149–155. [PubMed: 12033975]
- Efron N, Perez-Gomez I, Morgan PB. Confocal microscopic observations of stromal keratocytes during extended contact lens wear. *Clin. Exp. Optom* 2002b;85:156–160. [PubMed: 12033976]
- Erie JC. Corneal wound healing after photorefractive keratectomy: a 3-year confocal microscopy study. *Trans. Am. Ophthalmol. Soc* 2003;101:293–333. [PubMed: 14971584]
- Erie JC, Nau CB, McLaren JW, Hodge DO, Bourne WM. Long-term keratocyte deficits in the corneal stroma after LASIK. *Ophthalmology* 2004;111:1356–1361. [PubMed: 15234137]
- Erie JC, Patel SV, McLaren JW, Hodge DO, Bourne WM. Keratocyte density in the human cornea after photorefractive keratectomy. *Arch. Ophthalmol* 2003;121:770–776. [PubMed: 12796246]
- Erie JC, Patel SV, McLaren JW, Hodge DO, Bourne WM. Corneal keratocyte deficits after photorefractive keratectomy and laser in situ keratomileusis. *Am. J. Ophthalmol* 2006;141:799–809. [PubMed: 16545332]
- Erie JC, Patel SV, McLaren JW, Maguire LJ, Ramirez M, Bourne WM. Keratocyte density in vivo after photorefractive keratectomy in humans. *Trans. Am. Ophthalmol. Soc* 1999;97:221–236. [PubMed: 10703126]discussion 236-40
- Erie JC, Patel SV, McLaren JW, Nau CB, Hodge DO, Bourne WM. Keratocyte density in keratoconus. A confocal microscopy study(a). *Am. J. Ophthalmol* 2002;134:689–695. [PubMed: 12429244]
- Frueh BE, Cadez R, Bohnke M. In vivo confocal microscopy after photorefractive keratectomy in humans. A prospective, long-term study. *Arch. Ophthalmol* 1998;116:1425–1431. [PubMed: 9823340]
- Hollingsworth J, Perez-Gomez I, Mutalib HA, Efron N. A population study of the normal cornea using an in vivo, slit-scanning confocal microscope. *Optom. Vis. Sci* 2001;78:706–711. [PubMed: 11700964]
- Imre L, Resch M, Nagymihaly A. In vivo confocal corneal microscopy after keratoplasty. *Ophthalmologie* 2005;102:140–146. [PubMed: 15378334]
- Jalbert I, Stapleton F. Effect of lens wear on corneal stroma: preliminary findings. *Aust. N. Z. J. Ophthalmol* 1999;27:211–213. [PubMed: 10484194]
- Kallinikos P, Efron N. On the etiology of keratocyte loss during contact lens wear. *Invest. Ophthalmol. Vis. Sci* 2004;45:3011–3020. [PubMed: 15326115]
- Kallinikos P, Morgan P, Efron N. Assessment of stromal keratocytes and tear film inflammatory mediators during extended wear of contact lenses. *Cornea* 2006;25:1–10. [PubMed: 16331033]
- Kitzmann AS, Winter EJ, Nau CB, McLaren JW, Hodge DO, Bourne WM. Comparison of corneal endothelial cell images from a noncontact specular microscope and a scanning confocal microscope. *Cornea* 2005;24:980–984. [PubMed: 16227846]
- Lin L. A concordance correlation coefficient to evaluate reproductivity. *Biometrics* 1989;45:255–268. [PubMed: 2720055]
- McLaren JW, Nau CB, Kitzmann AS, Bourne WM. Keratocyte density: comparison of two confocal microscopes. *Eye Contact Lens: Sci. Clin. Prac* 2005;31:28–33.
- McLaren J, Nau CB, Patel SV, Bourne WM. How precisely can we determine keratocyte density by confocal microscopy? *Invest. Ophthalmol. Vis. Sci* 2001;42:S281.
- Mikek K, Hawlina M, Pfeifer V. Comparative study of human keratocyte density after corneal grafting by using confocal microscopy *in vivo*. *Klin. Monatsbl. Augenheilkd* 2003;220:830–834. [PubMed: 14704938]
- Mitooka K, Ramirez M, Maguire LJ, Erie JC, Patel SV, McLaren JW, Hodge DO, Bourne WM. Keratocyte density of central human cornea after laser in situ keratomileusis. *Am. J. Ophthalmol* 2002;133:307–314. [PubMed: 11860965]
- Moller-Pedersen T. A comparative study of human corneal keratocyte and endothelial cell density during aging. *Cornea* 1997;16:333–338. [PubMed: 9143808]
- Moller-Pedersen T. Keratocyte reflectivity and corneal haze. *Exp. Eye Res* 2004;78:553–560. [PubMed: 15106935]

- Moller-Pedersen T, Cavanagh HD, Petroll WM, Jester JV. Stromal wound healing explains refractive instability and haze development after photorefractive keratectomy: a 1-year confocal microscopic study. *Ophthalmology* 2000;107:1235–1245. [PubMed: 10889092]
- Mustonen RK, McDonald MB, Srivannaboon S, Tan AL, Doubrava MW, Kim CK. Normal human corneal cell populations evaluated by *in vivo* scanning slit confocal microscopy. *Cornea* 1998;17:485–492. [PubMed: 9756442]
- Patel SV, McLaren JW, Camp JJ, Nelson LR, Bourne WM. Automated quantification of keratocyte density by using confocal microscopy *in vivo*. *Invest. Ophthalmol. Vis. Sci* 1999;40:320–326. [PubMed: 9950589]
- Patel S, McLaren J, Hodge D, Bourne W. Normal human keratocyte density and corneal thickness measurement by using confocal microscopy *in vivo*. *Invest. Ophthalmol. Vis. Sci* 2001;42:333–339. [PubMed: 11157863]
- Patel SV, McLaren JW, Hodge DO, Bourne WM. Confocal microscopy *in vivo* in corneas of long-term contact lens wearers. *Invest. Ophthalmol. Vis. Sci* 2002;43:995–1003. [PubMed: 11923239]
- Perez-Gomez I, Efron N. Change to corneal morphology after refractive surgery (myopic laser in situ keratomileusis) as viewed with a confocal microscope. *Optom. Vis. Sci* 2003;80:690–697. [PubMed: 14560119]
- Pisella PJ, Auzeur O, Bokobza Y, Debbasch C, Baudouin C. Evaluation of corneal stromal changes *in vivo* after laser in situ keratomileusis with confocal microscopy. *Ophthalmology* 2001;108:1744–1750. [PubMed: 11581044]
- Popper M, Morgado AM, Quadrado MJ, Van Best JA. Corneal cell density measurement *in vivo* by scanning slit confocal microscopy: method and validation. *Ophthalmic Res* 2004;36:270–276. [PubMed: 15583433]
- Prydal JI, Franc F, Dilly PN, Kerr Muir MG, Corbett MC, Marshall J. Keratocyte density and size in conscious humans by digital image analysis of confocal images. *Eye* 1998;12:337–342. [PubMed: 9775227]
- Vanathi M, Tandon R, Sharma N, Titiyal JS, Pandey RM, Vajpayee RB. *In-vivo* slit scanning confocal microscopy of normal corneas in Indian eyes. *Ind. J. Ophthalmol* 2003;51:225–230.
- Vesaluoma M, Perez-Santonja J, Petroll WM, Linna T, Alio J, Tervo T. Corneal stromal changes induced by myopic LASIK. *Invest. Ophthalmol. Vis. Sci* 2000;41:369–376. [PubMed: 10670464]

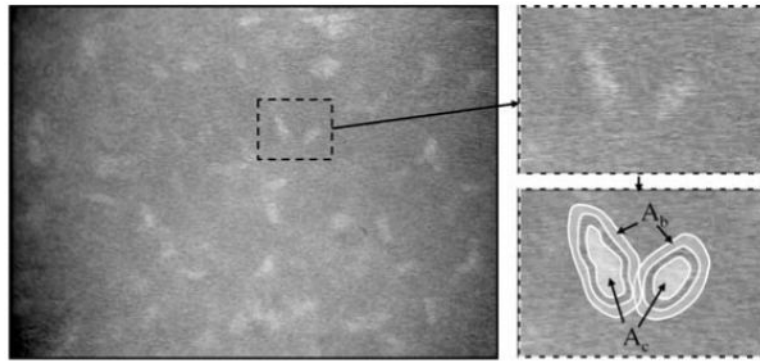


Fig. 1. Confocal image of normal mid-stroma. Bright objects represent nuclei, presumably of keratocytes. The subregion around two nuclei is magnified to the right. The areas A_c and A_b are the mask areas of each cell and background respectively, selected by the program. The input or processed image intensities under these areas were used to calculate variables, such as the brightness-area-product and contrast, and these were used to select objects that most likely represented cells.

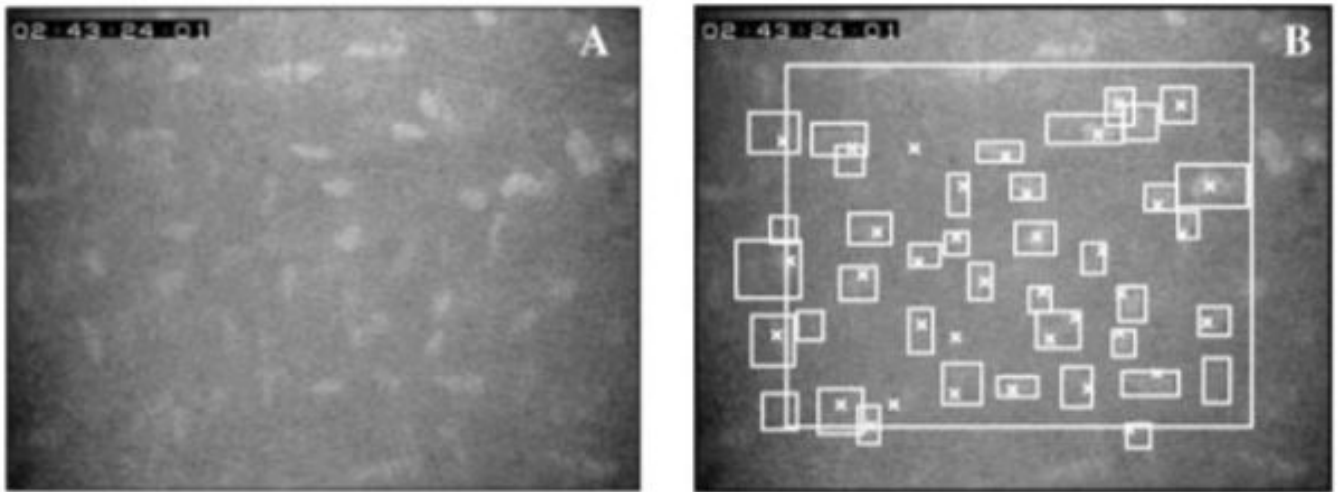


Fig. 2.

One confocal image before (A) and after counting cells (B). Cells were counted manually within or touching the left or bottom edge of the large rectangle and were indicated with an X. Cells identified by the program were indicated by a bounding box, the smallest rectangle with vertical and horizontal sides that entirely contained the cell. Most cells were identified by both methods, although some were identified by one or the other but not both.

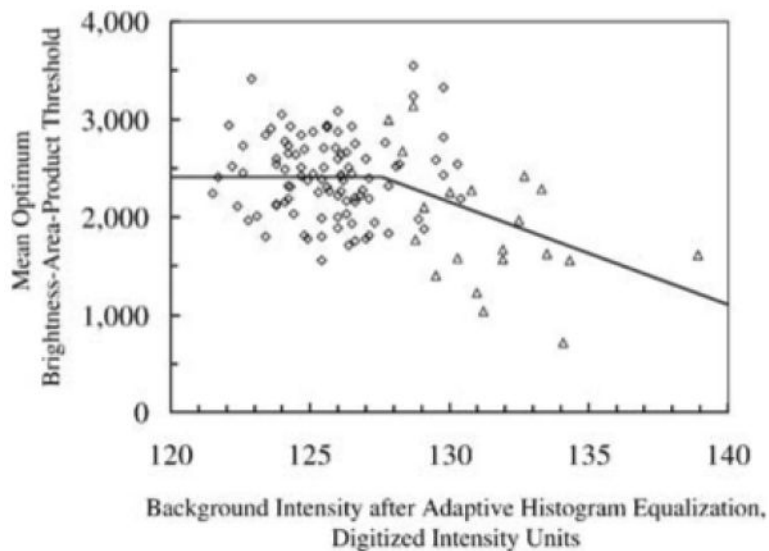


Fig. 3.

Relationship between mean optimum brightness-area-product threshold (\overline{BAP}_{thr}) and mean background intensity after adaptive histogram equalization (\overline{I}_{b-ahc}). Each marker represents the mean across all frames in a scan. The solid line represents the relationship that was used to determine the \overline{BAP}_{thr} for a particular scan when \overline{I}_{b-ahc} was calculated from the images. When \overline{I}_{b-ahc} was less than 128, \overline{BAP}_{thr} was constant (2411), and otherwise it was equal to $\overline{I}_{b-ahc} \times m_1 + b_1$ (Eq. 4), where m_1 and b_1 are given in Table 3. The coefficients m_1 , b_1 , and the transition intensity changed after March 1, 1999 (data shown were from scans after this date).

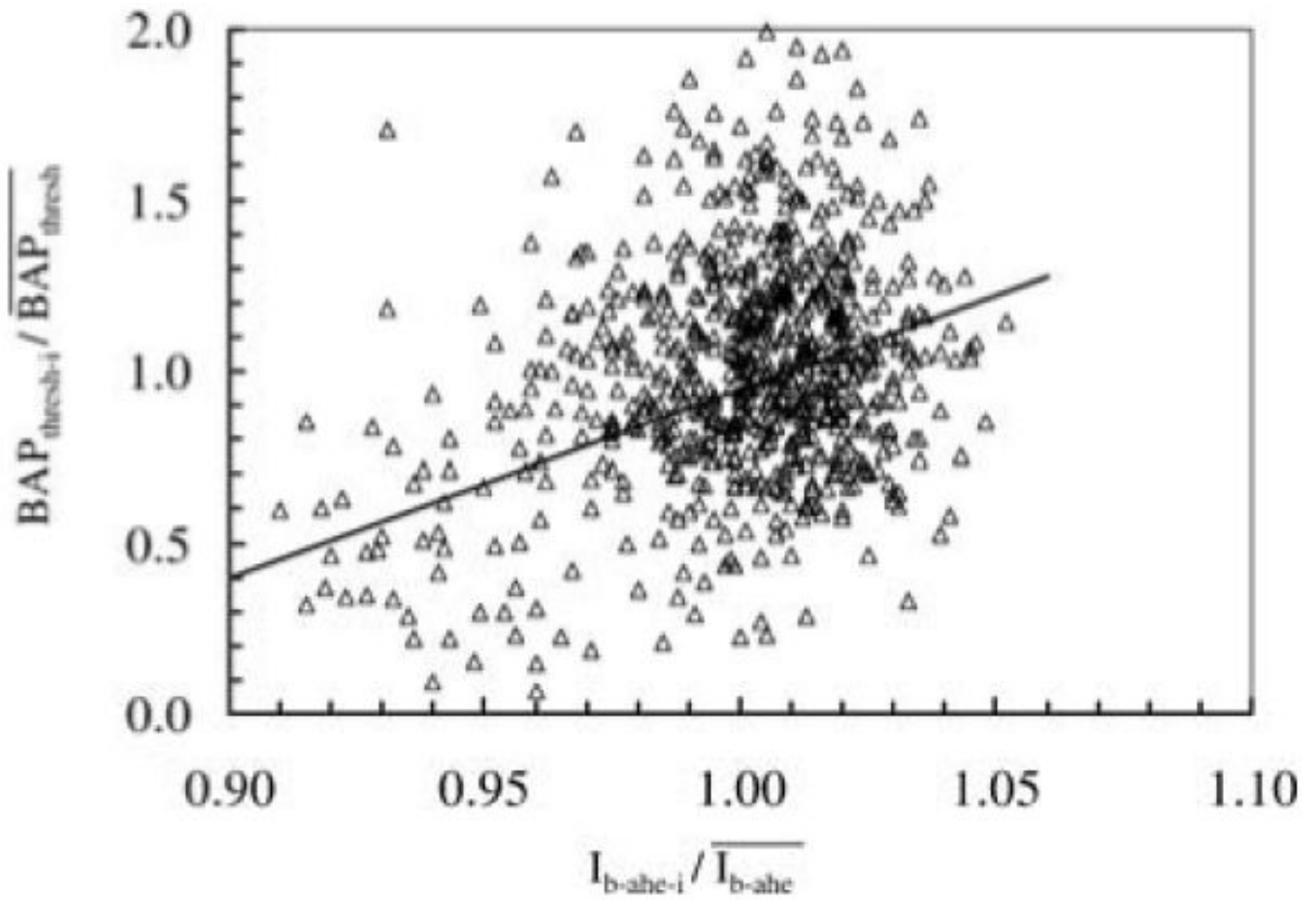


Fig. 4. Relationship used to adjust the BAP threshold in individual frames within a scan. Each marker represents data from one frame, and all frames were from normal control corneas described in Methods. The BAP threshold for a particular frame was determined from properties of the image by using Eq. (4) (solid line).

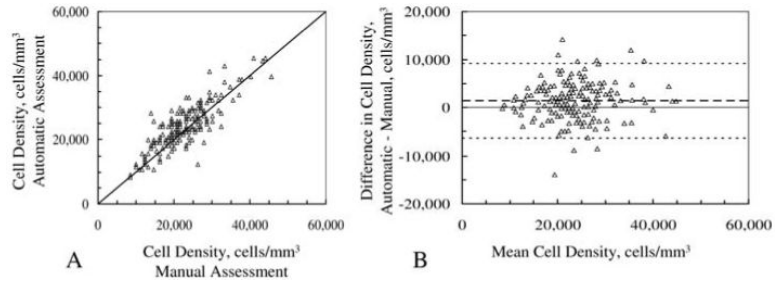


Fig. 5.

Relationship between automatic and manual assessments of cell density in 16 corneas 5 years after LASIK. Each marker represents densities from one frame. A, correlation between cell densities by automated and manual methods; solid line is identity line. B, difference in estimated cell density between methods vs. mean of both methods, as described by Bland and Altman (Bland & Altman, 1986). Dashed lines represent the limits of agreement, the mean difference \pm 2 standard deviations.

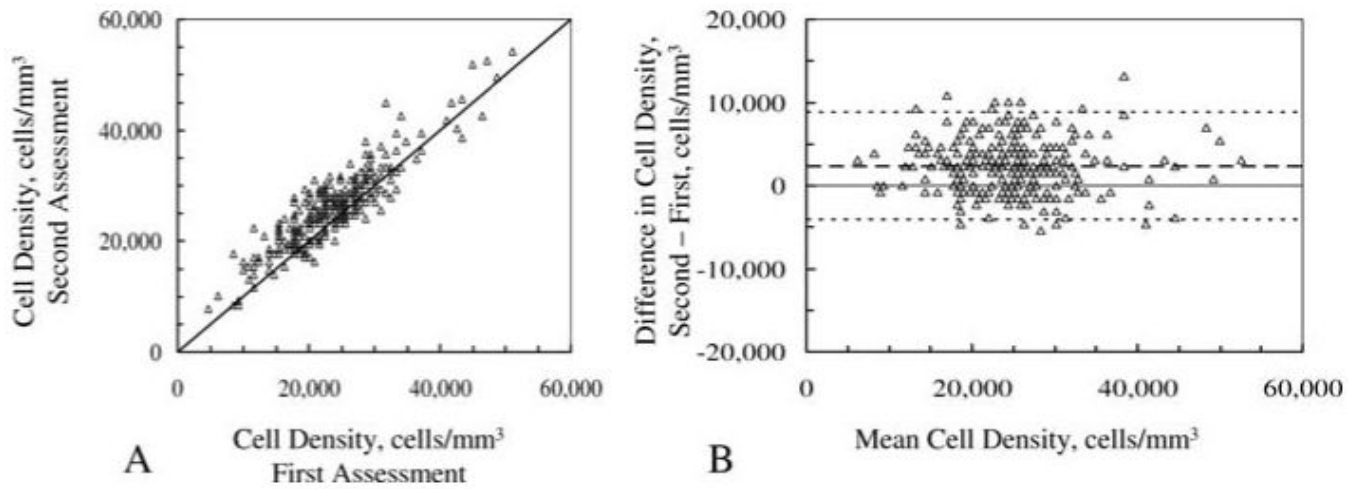


Fig. 6. Cell density estimated in same frames by one reviewer in two sessions. A, correlation between two manual assessments of cell density; solid line is identity line. B, difference vs. mean of estimates and limits of agreement. Scans were selected from those recorded 2 and 3 years after LASIK. Variation of differences in two estimates of cell density was similar to variation of differences between one observer and the program (Fig. 5).

Table 1

Steps used to identify objects in confocal images of the corneal stroma

Step	Process	Purpose
1	Inhomogeneity correction	Adjust local brightness to make brightness uniform across field.
2	Sigma filter	Reduce high-frequency noise.
3	Adaptive histogram equalization and low-pass filter	Redistribute intensities in image uniformly across full intensity range.
4	Threshold, 70% full range	Convert to binary image.
5	Mathematical morphology	Remove very small objects (noise), smooth edges of large objects, open bridges, and close gaps.
6	Subdivide each object	Separate cells that overlap (Table 2).
7	Sort objects by size	Objects can be addressed individually. Each object can be used as a mask to the original or processed images.

Table 2
Steps to subdivide overlapping objects (expansion of step 6 in Table 1)

Step	Process	Purpose
6a	Select region slightly larger than each object	Operate on subimage.
6b	Mask object in Adaptive Histogram Equalization image	Select object after adaptive histogram equalization (step 3).
6c	Low-pass filter	Reduce noise, smooth peaks and valleys.
6d	Adaptive histogram equalization	Redistribute intensities of cell; increase contrast.
6e	Threshold, 70% full range	Convert to binary.
6f	Homotopic thicken to original cell mask	Thicken objects without allowing them to merge.

Table 3
 Summary of parameters used to determine the optimum brightness-area-product threshold in Eq. (4)

Criteria for selection	$\bar{I}_{b-ahc} < \text{Boundary}$	$\bar{I}_{b-ahc} \geq \text{Boundary}$			Eq. (5)	
	BAP _{thr}	Boundary, I_{b-min}	m_1	b_1	M_2	b_2
Before March 1, 1999	2411	126.1	-226	30916	7.652	-6.667
After March 1, 1999	2411	128.2	-106	15913	5.477	-4.529

Mean full-thickness cell densities (unweighted for distance between frames) estimated by manual and automatic methods at each examination before and after LASIK

Table 4

	Mean Cell Density, cells/mm ³ Mean ± SD									
	Pre-LASIK	1 month	3 months	6 months	1 year	2 years	3 years	5 years		
Number of patients	17	17	17	17	17	15	17	16		
Manual	32765 ± 3944	28114 ± 4193	28338 ± 4246	28903 ± 2,326	27492 ± 3568	26038 ± 2881	26195 ± 1739	22920 ± 1728		
Automatic	31422 ± 3564	27696 ± 2399	28130 ± 3258	27368 ± 2161	25500 ± 2333	26460 ± 1755	25139 ± 2554	24311 ± 2276		
Difference	-1343 ± 3047	-418 ± 3898	-208 ± 2997	-1535 ± 2525	-1993 ± 3575	422 ± 2228	-1056 ± 1503	1392 ± 1780		
Difference as percent of manual	-4.1	-1.5	-0.7	-5.3	-7.2	1.6	-4.0	6.1		
P: *	0.06	0.19	0.80	0.02	0.007	0.44	0.02	<0.001		
MDD: ^a	1857	1776	2030	-	-	1534	-	-		

* Probability, generalized estimating equation models

^aMDD : minimum detectable difference, cells mm⁻³, based on generalized estimating equation models, $\alpha = 0.05$, $\beta = 0.20$.

Significance of difference between cell density after LASIK and density before LASIK

	Significance of difference in cell density from pre-LASIK						
	1 month	3 months	6 months	1 year	2 years	3 years	5 years
Manual Assessment							
Anterior flap	0.0009	0.0008	0.0006	<0.0001	<0.0001	<0.0001	<0.0001
Posterior flap	<0.0001	0.0005	<0.0001	<0.0001	<0.0001	<0.0001	<0.0001
Anterior RAZ	0.0029	0.0015	<0.0001	<0.0001	<0.0001	<0.0001	<0.0001
Posterior RAZ	0.0037	ns	ns	ns	ns	0.0044	<0.0001
66-90%	0.0054	ns	ns	0.0059	ns	0.0057	<0.0001
90-100%	ns	ns	ns	ns	0.0002	ns	0.0004
Automatic Assessment							
Anterior flap	<0.0001	<0.0001	<0.0001	<0.0001	<0.0001	<0.0001	<0.0001
Posterior flap	<0.0001	<0.0001	<0.0001	<0.0001	<0.0001	<0.0001	<0.0001
Anterior RAZ	ns	ns	ns	0.0001	0.0021	0.0003	<0.0001
Posterior RAZ	ns	ns	ns	ns	ns	ns	ns
66-90%	ns	ns	ns	0.0059	ns	ns	<0.0001
90-100%	ns	ns	ns	ns	ns	ns	ns

ns = not significantly different (Generalized estimating equation models, Bonferroni correction for seven comparisons, $P > 0.05/7$).

Table 6

Mean cell density in three assessments by one observer

Assessment	Auto	First	Second	Third
Cell density, cells mm ⁻³ (\pm SD)	24829 \pm 6866	22956 \pm 6676	26116 \pm 6221	23171 \pm 6788
Difference in density, cells mm ^{-3a}				
Auto		1874* \pm 4078	-1286** \pm 4187	1659* \pm 4027
First			-3160* \pm 2947	-215 \pm 3122
Second				-2945* \pm 2772

In all assessments n = 108 frames from nine corneas, 3 years after LASIK.

* $P < 0.0001$, paired t-test.

** $P = 0.002$, paired t-test.

^a Difference in density by assessment indicated in row minus density by assessment indicated in column.